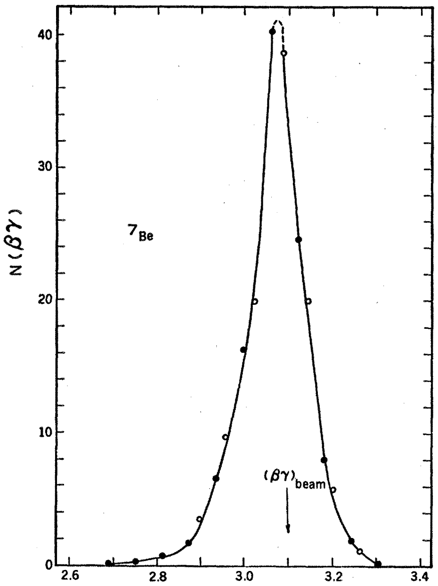

Fig. 3. Spectral line of the ^{7}Be isotope, uncorrected for energy loss in the target and resolution of the detector-spectrometer system. The arrow indicates the value of $\beta\gamma$ for the incident ^{14}N beam. The symbol β represents the velocity of the particle divided by the velocity of light, and γ is defined by the equation $\gamma = (1 - \beta^2)^{-1/2}$. The ordinate N is the number of counts observed as a function of $\beta\gamma$.

of the fragmentation products. The distance between the target and the particle identifier was approximately 40 m. Our first observations demonstrated that the 0° fragmentation products are predominantly due to the distintegration of the ^{14}N nucleus. This characteristic feature of the fragmentation process has been documented in studies of the interactions of cosmic-ray heavy ions by use of the nuclear emulsion technique (*2*). Virtually all the fragments heavier than helium (atomic number 2) have velocities that differ very little from the velocity of the beam. Qualitatively, the ^{14}N nucleus appears to simply fall apart, with the resultant nuclear products proceeding on with little or no change in velocity. The consequence of this fact is that, as one varies the rigidity R of the particles transmitted by the magnetic spectrometer, the intensity of a fragment of mass M and atomic number Z exhibits a sharp maximum when $R = (M/Ze)\beta\gamma$, where $\beta\gamma = \beta(1 - \beta^2)^{-1/2} \equiv (\beta\gamma)_{\rm beam}$. In these equations, e is the electron charge and β is the velocity of the particle divided by the velocity of light. The atomic number of the fragment is measured by the ion's rate of energy loss in traversing the counter telescope. The rigidity R has units Gv when the mass M is expressed in Gev.

We illustrate this in Fig. 1, where we show the spectra of elements produced in a carbon target at an angle of 0° when R was set at 5.0 and 6.2 Gv. (The rigidity of the 2.1-Gev/nucleon ^{14}N beam is 5.8 Gv.) In Fig. 1a, the prominent feature is the $Z = 4$, or beryllium, peak. Assuming that it is due to ^{7}Be, we find that the $\beta\gamma$ of this nuclide is 3.06, which is only slightly less than $(\beta\gamma)_{\rm beam} = 3.10$. When R is 6.2 Gv (Fig. 1b) the intensity of beryllium vanishes and carbon, $Z = 6$, dominates. Because 6.2 Gv is greater than the rigidity of the beam, no ^{14}N ions are observed. It follows that no ^{12}C can be present, since these ions have the same rigidity as ^{14}N at equal velocities. The $Z = 6$ peak at rigidity 6.2 Gv is therefore due to ^{13}C, which has, at this rigidity, a $\beta\gamma$ of 3.07—again equal to that of the incident ^{14}N beam.

These and subsequent measurements can be interpreted in terms of Fig. 2, where we have plotted the values of rigidity R for several isotopes of atomic numbers 1 through 8 under the assumption that their velocities are equal and hence that their $\beta\gamma$'s are equal to $(\beta\gamma)_{\rm beam}$ or 3.1. For orientation purposes, we indicate by arrows the points $R = 5.0$ and 6.2 Gv, appropriate for Fig. 1. An examination of the raw data has revealed the production of all the isotopes shown in Fig. 2 with mass number $A \leqq 14$ nucleons, excepting oxygen, within the rigidity interval 4.1 to 6.7 Gv—a limitation set by the spectrometer system. The observation of ^{14}C is evidence that charge exchange interactions also occur between the incident ^{14}N and the target nuclei.

To demonstrate the shape of a "spectral line" of an isotope, we show in Fig. 3 the measured intensity of ^{7}Be as a function of $\beta\gamma$. The maximum intensity occurs at $(\beta\gamma)_{\rm beam} = 3.1$ to the accuracy of these measurements. The width of the distribution is an upper limit of the natural width since these preliminary data have not been corrected for the resolution of the detector-spectrometer system.

HARRY H. HECKMAN
Lawrence Berkeley Laboratory, University of California, Berkeley 94720
DOUGLAS E. GREINER
PETER J. LINDSTROM
FREDERICK S. BIESER
Space Sciences Laboratory, University of California, Berkeley

References and Notes

1. H. A. Grunder, W. D. Hartsough, E. J. Lofgren, *Science* **174**, 1128 (1971).
2. C. F. Powell, P. H. Fowler, D. H. Perkins, *The Study of Elementary Particles by the Photographic Method* (Pergamon, New York, 1959), pp. 579–640.
3. Work done under the auspices of the Atomic Energy Commission and under NASA grant NGR-05-003-405.

24 September 1971

Radiological Physics Characteristics of the Extracted Heavy Ion Beams of the Bevatron

Abstract. *Studies of the depth-ionization properties and the biological effects of heavy ion beams produced at the bevatron have extended work previously done with less energetic beams from other sources. Results indicate that heavy ion beams are suitable for tumor therapy, studies relating to space biology, and fundamental radiobiology.*

Recently achieved nitrogen beams of a few hundred million electron volts per nucleon at the bevatron (*1, 2*) have given us an opportunity to investigate the radiological properties of these particles and make an initial assessment of the potential usefulness of still heavier ions for future biological investigations in medical therapy. Since the completion of the first synchrocyclotron at Berkeley in 1947, we have conducted biophysical investigations with accelerated protons, deuterons, and helium ions, and also, since completion of the heavy ion linear accelerator (Hilac) about 14 years ago, with low-energy (less than 10 Mev/nucleon) heavy ions, including argon beams. These studies indicate that the high linear energy transfer of the particles might be particularly suitable for therapy of certain types of tumors since they produce similar effects on anoxic tumor cells and on oxygenated normal cells. This is unlike low linear energy transfer radiations, that is, x-rays, which kill normal oxygenated cells preferentially. Furthermore, it was predicted that the depth-ionization properties of heavy ion beams producing a peak (Bragg ionization curve) may make penetrating monoenergetic beams particularly suitable for producing well-localized radiolesions in multicellular organisms without surgical trauma and bleeding (*3–5*).

The deflected nitrogen and helium ion beams from the bevatron were collimated by magnetic focusing to a slowly divergent cone with a beam cross section of 0.6 by 1.5 cm^2 at the apex, where the experimental studies were performed. The depth-ionization properties of the beams were studied by means of ionization chambers and fast plastic scintillators. As shown in Fig. 1, a beam was monitored by thin-blade plastic scintillators and an ion chamber (I1) constructed of thin parallel aluminum foils. This apparatus is similar to that used in therapeutic investigations with beams of heavy charged particles (*6*). The beam was then passed through a variable thickness water column with Lucite windows; energy transfer in the water column is similar to that in tissue. The thickness of the water absorber could be remotely controlled during the measurements. A second ionization chamber (I2) adjacent to the water absorber monitored ionization due to the particles after they passed through the water column. The normalized ratio of the charge collected in I2 to that collected simultaneously in I1 when the nitrogen beam passed through them was measured as a function of the thickness of the water absorber.

Thus, we obtained the Bragg ionization curve for nitrogen, shown in Fig. 1. The range of the particles calculated from these data corresponds to that of a nearly monoenergetic nitrogen beam of about 278 Mev/nucleon. The shape of the ionization curve corresponds closely to that predicted by Steward (*7*) and Litton (*8*). The beam was deflected from the accelerator in a pulse of about 1-msec duration; it is calculated that the energy spread of the deflected beam might have been as much as 1.5 Mev/nucleon; this would account for most of the spread in range of the particles. Straggling and multiple scattering are less important in this respect than the initial energy spread of the beam. Thus, it is possible that the Bragg ionization peak of a truly monoenergetic beam is even higher than observed. The measured ionization values are proportional to the distribution of dose in soft tissue. From a plateau, the ionization ratio rises near the end of the particles' range to a peak at about 5.82 before it drops to a low value, about 15 percent of the plateau value. The sharp rise of the Bragg ionization curve indicates that it should be possible to produce deep lesions at specific locations inside the human body, as required by therapeutic need, with minimal hazard of hemorrhage.

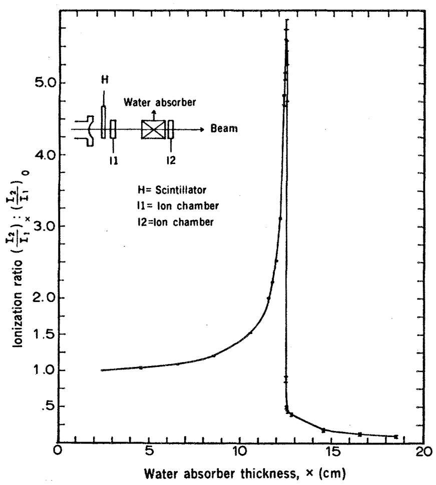

Fig. 1. Diagram represents the apparatus used to obtain the Bragg ionization curve. The parallel plate ionization chambers I1 and I2 are filled with nitrogen gas; their diameters are 12.7 and 7.6 cm, respectively. A variable absorber is interposed between the ion chambers to allow measurement at thickness x of the ratio $(I2/I1)_x$. The data are normalized by forming the ionization ratio $(I2/I1)_x : (I2/I1)_0$.

The Bragg ratio (the ratio of the ionization peak value to its plateau value) is significantly better than that of high-energy protons, deuterons, or helium ions (*8*). In depth-dose characteristics, the nitrogen beams compare favorably with other radiations used in radiation therapy or proposed for such use. This is illustrated in Fig. 2, where the relative depth ionization of various radiations is given. The curve for pi-mesons of 65-Mev kinetic energy is based on measurements by Raju and Richman (*9*). For comparison, an absorption curve for cobalt gamma rays and a depth-dose curve for 14.6-Mev neutrons are given (*10, 11*). The depth-dose advantages of nitrogen beams for the production of localized lesions are obvious from the graph. The use of nitrogen beams is also advantageous for the irradiation of larger regions, and broad depth-dose distributions can be achieved by using beams with varying momentum spreads. In assessing various radiations for radiation therapy, a distinction should be made between actual measured properties (such as those given in Fig. 2) and theoretical estimates, which often include assumed or calculated quantities such as radiation-equivalent-man values (*3, 12, 13*).

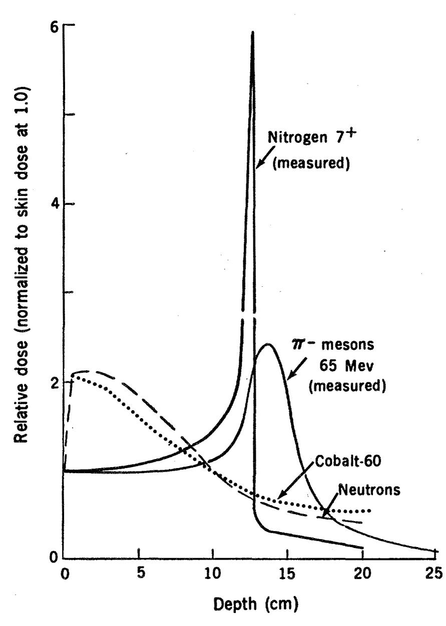

Fig. 2. Depth-dose curves for 278 Mev/nucleon nitrogen-14 ions in water, 65-Mev π^- mesons (*9*), cobalt-60 gamma rays (*10*), and 14.6-Mev neutrons (*11*), all normalized to skin entrance dose. The nitrogen beam is monoenergetic, whereas the mesons correspond to about an energy spread of several million electron volts.

The portion of the depth-ionization curve beyond 12.55 cm in Fig. 1 is due to secondary particles generated by collisions of the nitrogen ions with nuclei of the absorber and to (less than 5 percent) contaminating protons and helium ions. The secondary particles have been identified by particle spectroscopy with lithium-silicon detectors as nuclei of atomic numbers 4 to 7. These nuclei stop in the vicinity of the nitrogen particles' Bragg ionization peak and thus contribute to the dose in the peak. Secondary protons and helium ions have longer ranges and contribute to ionization only in minor ways. The contribution of secondary neutrons is even smaller. These secondaries do not diminish the usefulness of nitrogen beams in research or in therapeutic applications. It appears that calculations made by Curtis (*14*) for secondaries in beams of neon ions are also valid. It is possible that combinations of neon or of nitrogen beams of several energies will yield depth-dose distributions that are flexible and controlled and suitable for tumor therapy.

The stopping of the particles was also studied by a method in which the particles were individually counted. The general layout for this experiment is shown in Fig. 3. It consists of the plastic scintillators for monitoring the impinging high-energy beam, the variable water absorber, and two thin scintillation monitors for the emerging beam (each having a stopping power approximately equivalent to that of 3.5 mm of water). At various absorber thicknesses, we obtained single counts of the monitor S_1, coincidence between S_1 and S_2, and triple coincidences between S_1, S_2, and S_3. Figure 3 contains a graph of some of the data, which are normalized and corrected for additional absorbers in front of the experimental setup within the beam. Pulse-height discrimination was applied in such a manner that most of the lighter secondary fragments such as protons and helium ions, which usually have a lower rate of ionization than primary nitrogen particles, were not recorded. Some of the heavier fragments, for example, boron and carbon, are probably included in the measurements. The initial slope of the curve and the exit portion are strongly affected by discrimination settings, but the rapid drop at the end of the range is not affected. Most of the nitrogen particles stopped very abruptly at an absorber equivalent to 12.55 cm of water. The shapes of the curve in Fig. 1 and the upper curve in Fig. 3 are in good agreement with theoretical results (*7, 8*). Figure 3 includes a graph of the differential stopping data, which indicates the number of particles that stop in scintillator S_2. Values for this graph were obtained by subtracting triple coincidences (S_1, S_2, S_3) from double coincidences (S_1, S_2).

Inelastic collisions of the high-speed nitrogen beam produce nuclear fragmentation. The fragments of the nitrogen particles keep traveling forward with about the same velocity as the particles of the primary beam. This was clearly shown in the experiments of Heckman *et al.* (*1*) with nitrogen beams of 2 Gev/nucleon. Using the nitrogen beams of 278 Mev/nucleon, we have obtained evidence that the fragments of nitrogen sometimes are radioactive nuclides. Because of the speed of the fragments, this radioactivity becomes deposited near the end of the range of the nitrogen beam, unlike the radioactivity produced by the beam in target nuclei, which is approximately uniformly distributed along the entire beam path. Using pure metallic beryllium as an absorber for the nitrogen beam and also as catcher for the radioactivity, we have obtained measurements of the distribution of radioactive ^{11}C and ^{13}N in the nitrogen beam. Since the radioactivity induced in beryllium is negligibly small, almost all of the radioactivity deposited is due to breakdown of the moving nitrogen nuclei. Some of the data are shown in Fig. 4; more details will be published (*15*). Thus, radioactivity produced by heavy particles in matter is representative not only of the composition of the target but also of the bombarding projectile. This statement has geophysical implications. For example, we expect that over long time periods heavy primary cosmic rays (consisting of nitrogen and heavier nuclei) have produced radioactive ^{14}C

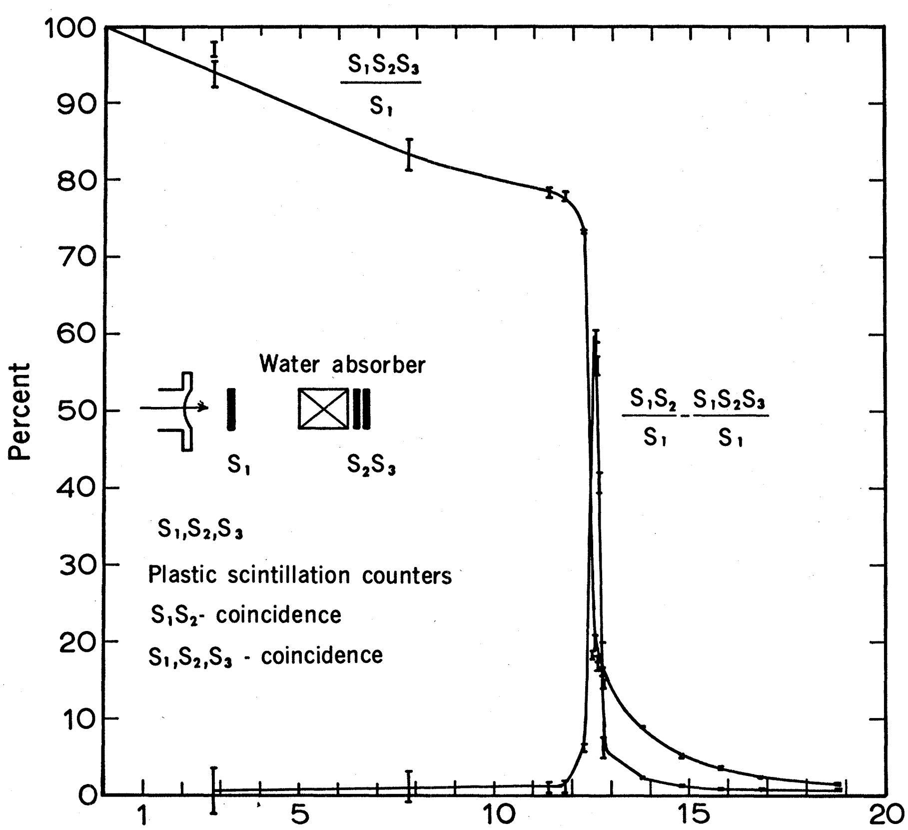

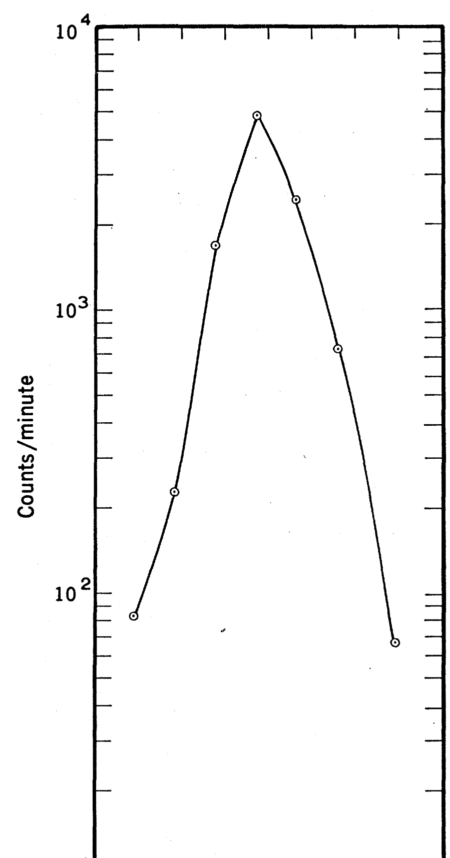

Fig. 3 (left). Number-distance relationship (upper curve) and differential range curve (lower curve) for 278-Mev/nucleon ^{14}N ions in water. Three plastic scintillators, S_1, S_2, and S_3, are arranged as shown above with a variable water absorber behind S_1. The percent of particles that pentrate all three scintillators is given by $(S_1S_2S_3/S_1) \times 100$. The quantity $[(S_1S_2/S_1) - (S_1S_2S_3/S_1)] \times 100$ describes the number of particles in percent that stop in scintillator S_3 but pass through both S_1 and S_2. Fig. 4 (right). A 278-Mev N^{7+} beam was passed into a slab of pure beryllium (*Be*) metal and was allowed to stop there at a depth of about 13 g cm^{-2}. Radioactive fragments of nitrogen produced in collisions with beryllium atoms were deposited near the end of the N^{7+} range. This graph shows the results of counting the ^{11}C gamma rays as a function of depth in beryllium.

and other long-lived isotopes in the lunar surface at depths related to the earth's atmosphere and beneath the penetration of the primary particles. Most of the long-lived radioisotopes in the earth's crust were incorporated at the time of the birth of the solar system. However, continuous creation of ^{40}K and of other isotopes occurs by the breakdown of cosmic-ray nuclei in the calcium to iron groups. The deposition of carrier-free ^{11}C fragments at the end of the range may be useful for medical research: external measurement of the location of the autoradioactive deposit might provide a convenient means for finding out (for example, in patients in vivo) where the beam has stopped, and the fate and transport of beam-deposited isotopes can be further studied with in vivo counting techniques.

Most of the studies described were performed in parallel with physical improvements on the bevatron for nitrogen beam acceleration. Although the beam intensity was relatively small, it was possible to carry out a few bioexperiments demonstrating the effects of small groups of particles. In working with T. Budinger, it was shown that the individual particles can produce a sensation of light flashes and streaks when they are aimed at the human retina, whereas nitrogen particles directed to the occipital lobes of the brain, where visual sensations are elaborated, failed to elicit light sensation (*16*). The effects observed are similar to those reported by astronauts in lunar flights. Measurements of the fluorescence of various fluids placed in the nitrogen beam—including rabbit vitreous fluid and retina—have demonstrated that the observed light flashes are probably due to direct excitation and ionization.

Preliminary measurements were made by members of our biomedical group (*17*) of survival curves, relative biological effectiveness (RBE), and "oxygen effect ratio" (OER) for mammalian kidney cells in culture (T1 cells). At the 10 percent survival level the OER is between 1.0 and 1.4 and the RBE is about 3. For 250-Mev nitrogen particles, at the 10 percent survival level the OER is between 1.9 and 2.4 and the RBE is about 1.5. These data are in general agreement with theoretical prediction for the oxygen effect of fast heavy ions (*5*); it would appear that nitrogen beams and still heavier ions, when used in radiation therapy, will reduce the oxygen effect more effectively than pimesons (*9*) or neutrons (*11*). The group has also exposed the skin of black mice (C57-BL) to small bursts of nitrogen particles, which were allowed to stop in skin. The development of bleached hair as a consequence is an indication of the profound effects of individual nitrogen particles on the pigment cells of the hair follicles (*17*).

The effects of single accelerated nitrogen ions have also been demonstrated by exposing maize to low doses (for example, 1 rad). About 5 percent of the developing plants from irradiated seeds exhibited gross malformations as compared to unirradiated controls, which did not exhibit these effects (*17*). The morphology of these effects seems to be peculiar to heavy ion irradiation.

C. A. Tobias, J. T. Lyman
A. Chatterjee, J. Howard
H. D. Maccabee, M. R. Raju
A. R. Smith, J. M. Sperinde
G. P. Welch

Donner Laboratory and *Lawrence Berkeley Laboratory, University of California, Berkeley 94720*

References and Notes

1. H. H. Heckman, D. E. Greiner, P. J. Lindstrom, F. S. Bieser, *Science* **174**, 1130 (1971).
2. H. A. Grunder, W. D. Hartsough, E. J. Lofgren, *ibid.*, p. 1128.
3. C. A. Tobias, J. T. Lyman, J. H. Lawrence, *Report UCRL-20802* (University of California Radiation Laboratory, Berkeley, 1971); in *Progress in Nuclear Medicine*, J. H. Lawrence, Ed. (Grune & Stratton, New York, in press), vol. 3.
4. C. A. Tobias and P. W. Todd, *Nat. Cancer Inst. Monogr.* **24**, 1 (1967).
5. C. A. Tobias, in *Symposium Papers of the Second International Conference on Medical Physics*, J. S. Laughlin and E. W. Webster, Eds. (International Conference on Medical Physics, Inc., Boston, 1971), pp. 28–50.
6. M. R. Raju, J. T. Lyman, T. Brustad, C. A. Tobias, in *Radiation Dosimetry* (Academic Press, New York, 1969), vol. 3, pp. 151–193.
7. P. G. Steward, *Report UCRL-18127* (University of California Radiation Laboratory, Berkeley, 1968).
8. G. M. Litton, *Report UCRL-17392* (University of California Radiation Laboratory, Berkeley, 1967).
9. M. R. Raju and C. Richman, *Gann Monogr. n9* (1970).
10. "Depth dose tables for use in radiotherapy," *Brit. J. Radiol.* **10** (Suppl.) (1961).
11. J. Broerse, G. W. Barendsen, G. R. Van Kersen, *Int. J. Radiat. Biol.* **13**, 559 (1967).
12. L. Rosen, *Science* **173**, 490 (1971).
13. G. W. Barendsen, *Eur. J. Cancer* **2**, 333 (1966).
14. S. B. Curtis, *Report UCRL-18347* (University of California Radiation Laboratory, Berkeley, 1968), pp. 171–174.
15. C. A. Tobias, A. Chatterjee, A. R. Smith, *Phys. Lett.* **37A**, 119 (1971).
16. C. A. Tobias and T. F. Budinger, *Report LBL-528* (Lawrence Berkeley Laboratory, Berkeley, Calif., 1971).
17. T. Budinger, A. Chatterjee, W. Heinze, J. Howard, J. Leith, J. Lyman, H. Maccabee, B. Martins, R. McGregor, M. Raju, A. Smith, M. Sperinde, C. Tobias, G. Welch, T. Yang, Y. Zeevi, *Report LBL-529* (Lawrence Berkeley Laboratory, Berkeley, Calif., 1971).
18. It is a pleasure for the authors to acknowledge the help and cooperation of many individuals, including the bevatron crew, F. Upham and the electronics group, R. Armer, and R. Walton. We are indebted to Dr. H. Heckman for the loan of his scintillator, and to Drs. J. L. Born and J. L. Lawrence for their encouragement throughout this work. This work was supported jointly by the Atomic Energy Commission and the National Aeronautics and Space Administration.

24 September 1971

Human Leukemic Cells: In vitro Growth of Colonies Containing the Philadelphia (Ph^1) Chromosome

Abstract. *Human leukemic cells with a marker (Philadelphia; Ph^1) chromosome gave rise to granulocytic and mononuclear cell colonies when grown in vitro. All metaphases from a single colony were either Ph^1 positive or Ph^1 negative. No colonies contained a mixed cell population. This suggests that leukemic and normal cells exist simultaneously and that in vitro colonies are clonal in origin.*

Colonies of granulocytes and mononuclear cells can be grown in vitro from bone marrow and blood of animals (*1, 2*) and man (*3–7*). Colonies can be grown from patients with various hematologic and nonhematologic diseases as well as from normal individuals (*3–7*). Colonies arising from human blood and marrow contain eosinophils, neutrophils, monocytes, or macrophages (*3*). In a number of instances, cells from patients with leukemia have been observed to give rise to similar colonies (*4, 6–8*). However, it has not been definitely established that these colonies arise from the leukemic cell population.

In approximately 90 percent of patients with typical chronic myelocytic leukemia (CML), a characteristic chromosome abnormality is present in cells arising in the marrow (*9, 10*). This abnormal marker, the Philadelphia or Ph^1 chromosome, has recently been identified as a G-22 autosome (*11*) with deletion of a substantial portion of its long arms. It is the only chromosomal marker consistently found in a human neoplasm and does not occur in any other disease, with the excep-